Induced-charge electrophoresis near a wall

Mustafa Sabri Kilic[1] and Martin Z. Bazant[1,2,3]
[1] *Department of Mathematics, Massachusetts Institute of Technology, Cambridge, MA 02139,USA*
[2] *Department of Chemical Engineering, Massachusetts Institute of Technology, Cambridge, MA 02139,USA and*
[3] *UMR Gulliver ESPCI-CNRS 7083, 10 rue Vauquelin, F-75005 Paris, France*
(Dated: December 29, 2010)

Induced-charge electrophoresis (ICEP) has mostly been analyzed for asymmetric particles in an infinite fluid, but channel walls in real systems further break symmetry and lead to dielectrophoresis (DEP) in local field gradients. Zhao and Bau (Langmuir, 23, 4053, 2007) predicted that a metal (ideally polarizable) cylinder is repelled from an insulating wall in a DC field. We revisit this problem with an AC field and show that attraction to the wall sets in at high frequency and leads to an equilibrium distance, where DEP balances ICEP, although, in three dimensions, a metal sphere is repelled from the wall at all frequencies. This conclusion, however, does not apply to asymmetric particles. Consistent with the experiments of Gangwal et al. (Phys. Rev. Lett., 100, 058302, 2008), we show that a metal/insulator Janus particle is always attracted to the wall in an AC field. The Janus particle tends to move toward its insulating end, perpendicular to the field, but ICEP torque rotates this end toward the wall. Under some conditions, the theory predicts steady translation along the wall, perpendicular to the field, at an equilibrium tilt angle around 45 degrees, consistent with the experiments, although improved models are needed for a complete understanding of this phenomenon.

I. INTRODUCTION

Most theoretical work on electrophoresis has focused on spherical particles moving in an infinite fluid in response to a uniform applied electric field [1–4]. Of course, experiments always involve finite geometries, and in some cases walls play a crucial role in electrophoresis. The linear electrophoretic motion of symmetric (spherical or cylindrical) particles near insulating or dielectric walls [5–10] and in bounded cavities or channels [11–20] has been analyzed extensively. Depending on the geometry and the double-layer thickness, walls can either reduce or enhance the translational velocity, and the rotational velocity can be opposite to the rolling typical of sedimention near a wall. The classical analysis for thin double layers assumes "force-free" motion driven by electro-osmotic slip alone, but recent work has shown that electrostatic forces can also be important near walls [21, 22]. Heterogeneous particles with non-uniform shape and/or zeta potential exhibit more complicated bulk motion [23–26], which can also affect boundary interactions [27], especially if the particles are deformable, as in the case of chain-like biological molecules [28].

In this article, we focus on the effect of nonlinear induced-charge electro-osmotic (ICEO) flows at polarizable surfaces, which are finding many new applications in microfluidics and colloids [29, 30]. The canonical example of quadrupolar ICEO flow around a polarizable particle, first described by Murtsovkin [31, 32], involves fluid drawn in along the field axis and expelled radially in the equatorial plane in an AC or DC field, and similar flows have been predicted [33, 34] and observed [35, 36] around metallic structures in microfluidic devices. Broken symmetries in this problem can generally lead to hydrodynamic forces and motion induced-charge electrophoresis (ICEP), as well as electrical forces and motion by dielectrophoresis (DEP). Until recently, such phenomena have only been analyzed for isolated asymmetric particles in an infinite fluid [33, 37, 38] or in a dilute solution far from the walls [39, 40]. In contrast, experiments demonstrating translational ICEP motion have involved strong interactions with walls [41, 42], which remain to be explained. Independently from an early preprint of this work [43], the first theoretical studies of wall effects in induced-charge electrophoresis were published by Wu, Gao and Li [44, 45], using similar models, applied to isotropic spherical particles.

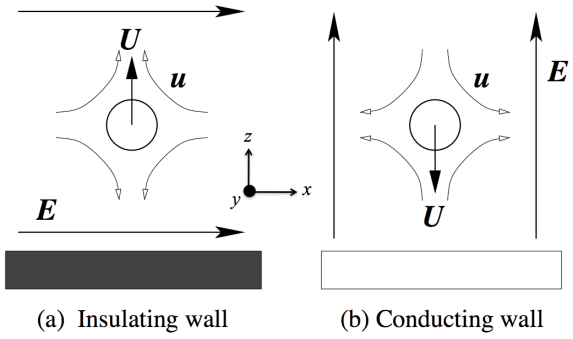

FIG. 1: Hydrodynamic forces on polarizable particles near (a) insulating and (b) unscreened conducting walls due to ICEO flows

As shown in Figure 1, it is easy to see that the quadrupolar ICEO flow around a polarizable particle typically causes attraction to unscreened conducting walls (perpendicular to the field) and repulsion from insulating walls (parallel to the field). The former effect of ICEP attraction to conducting walls has not yet been analyzed; it may play a role in colloidal self assembly on electrodes applying AC voltages [46–51]. This phenomenon is mainly

understood in terms of electrohydrodynamic flows (what we would term "ICEO") induced on the electrodes, not the particles (typically latex spheres), but ICEP could be important for more polarizable particles.

The latter effect of ICEP repulsion from insulating walls has been analyzed by Zhao and Bau [52] in the case of a two-dimensional ideally polarizable cylinder in a DC field, and by Wu, Gao and Li[44, 45] for a colloid of ideally polarizable spheres in a microchannel. To our knowledge, however, this phenomenon of wall repulsion has not yet been confirmed experimentally. On the contrary, Gangwal et al [42] have recently observed that metallo-dielectric Janus particles are attracted to a glass wall, while undergoing ICEP motion parallel to the wall and perpendicular to an applied AC field. It is not clear that the existing theory of ICEP can explain this surprising behavior.

The objective of this work is to analyze the motion of three-dimensional polarizable particles near insulating walls in AC fields. As summarized in section II, we employ the low-voltage "Standard Model" [53] in the thin double-layer approximation, following many authors [34, 35, 37, 38], including Zhao and Bau [52]. In section III, we first analyze ideally polarizable cylinders and spheres near a non-polarizable wall, which only experience forces perpendicular to the wall. In section IV we then study spherical metal/insulator Janus particles, which are half ideally polarizable and half non-polarizable. Due to their broken symmetry, the Janus particles also experience ICEP and DEP torques, which strongly affect their dynamics near the wall.

II. MATHEMATICAL MODEL

A. Low Voltage Theory

In this paper, we will consider either a cylindrical or a spherical particle of radius a in a semi-infinite electrolyte bounded by a plane. The closest distance between the particle and the plane is denoted by h. In the absence an applied electric field, we assume that the particle and the wall surfaces are uncharged. In addition, we will assume the electrolyte has a low Reynolds number, and impose the Stokes equations. We will assume that the thin double layer approximation holds and the bulk electrolyte remains electroneutral, which is the case when the Debye length

$$\lambda_D = \sqrt{\frac{\varepsilon kT}{2z^2e^2c_0}}$$

is much smaller than the characteristic length scale (in our case, a). The Debye length is less than $100nm$ in aqueous solutions, while colloidal particles and microchannels (as in the experiments considered below) are typically at the micron scale or larger. In such situations, the thin double layer approximation is thus well justified, except when particles come into very close contact with walls, as noted below.

Due to the mathematical complexity of particle motion near a wall, especially in the case of asymmetric Janus particles, we adopt the simple Standard Model for ICEO flows [30, 53], which assumes thin double layers, uniform bulk concentration, negligible surface conduction and surface or bulk reactions. Under these assumptions, the potential satisfies Laplace's equation

$$\nabla^2\phi = 0$$

and the fluid flow is governed by the Stokes equations

$$\eta\nabla^2\mathbf{u} = \nabla p, \quad \nabla\cdot\mathbf{u} = 0 \tag{1}$$

where ϕ is the electrostatic potential and ε the permittivity, η the viscosity of the electrolyte, $\mathbf{u}$ the velocity field and p the pressure.

Boundary conditions are critical in electrokinetic phenomena. The wall boundary $z = 0$ is a non-polarizable insulator, with vanishing normal field from the electrolyte,$\mathbf{n}\cdot\nabla\phi = 0$, whereas the particle surface, being polarizable, acts as a capacitor in the thin double layer limit [34, 54],

$$\frac{dq}{dt} = (-\mathbf{n})\cdot(-\kappa\nabla\phi)$$

where q is the surface charge density on the particle, κ the conductivity of the bulk electrolyte. Far away from the particle, an electric field parallel to the wall

$$\nabla\phi \sim \mathbf{E}_\infty = E_\infty\hat{\mathbf{x}}, \quad \text{as} \quad |\mathbf{x}| \to \infty$$

is applied. In general, the amplitude $E_\infty(t)$ is time dependent.

As a first approximation, we do not consider explicitly any effects of nonzero equilibrium charge on any of the surfaces in the system, beyond that which is induced by capacitive charging of the double layers in response to the applied field. On the polarizable particle surface of the particle, we thus neglect the possibility of charge regulation by specific adsorption/desorption of ions, which effectively contributes an additional interfacial capacitance, in parallel with the diffuse and compact parts of double layer, which has has recently helped to improve quantitative comparisons between theory and experiment for ICEO flows [36] and ACEO pumping [55, 56]. On the non-polarizable surfaces of the particle (in the case of a Janus particle) and the wall, we likewise neglect the effects of a nonzero equilibrium "fixed charge", most notably classical, linear electro-osmotic flow. In the limit of a steady DC applied field, these flows must be considered, if the equilibrium zeta potential on the non-polarizable surfaces (typically of order the thermal voltage, $kT/e \approx$ 25 mV) is comparable to the induced zeta potential on the polarizable surfaces (of order Ea or less), which corresponds to weak fields, $E < kT/ea = 0.1$ V/cm for a 2.5 μm particle.

Our main interest in this article, however, is to analyze particle dynamics under AC forcing, for which linear fixed-charge electro-osmotic flows average to zero, if there is enough time for double layer charging within one period [30, 34, 35]. In that case, it is justified to neglect the fixed charge on non-polarizable particle and wall surfaces, as long as the particle remains far enough from the wall to neglect direct electrostatic interactions (mediated by the electrolyte double layers), which survive time averaging. This assumption is consistent with the thin double layer approximation, the fixed charge is screened at separations exceeding the Debye length (< 100 nm in water). Larger separations are maintained in most situations involving symmetric particles, but our model predicts that in some cases, asymmetric Janus particles are driven to the wall by nonlinear electrokinetic effects, which lead to close approach by the non-polarizable surface of the particle, which is either enhanced to contact by electrostatic forces in the case of oppositely charged surfaces or halted by repulsion for like-charged surfaces (as in experiments [42]). For this reason, we close the article by commenting on possible effects of close electrostatic interactions, but otherwise we focus on the dynamics in the regime of thin double layers, where the particle-wall separation exceeds Debye length.

With these assumptions, the Stokes equations are supplied by the no-slip conditions on the wall and the Smoluchowski's electrokinetic slip formula on the polarizable surfaces of the particle

$$\mathbf{u} = \mathbf{u}_{slip} = \frac{\varepsilon}{\eta}\zeta \nabla_s \phi$$

where ζ is the potential difference between the surface and the bulk. Lastly, we assume that the flow vanishes far from the particle.

So far, the equations are complete except for a constitutive relation between ζ and q on the polarizable surface. In the regime of small induced voltages ($e\zeta \ll kT$), the general nonlinear charge-voltage relation takes the simple linear form,

$$q = -\frac{\varepsilon}{\lambda_D}\zeta$$

although the complete problem is still nonlinear in this case because of the quadratic slip formula (6). In this paper, we will study only the linear response of the double layer, but the calculations can be repeated with (sometimes more accurate) nonlinear theories [53, 57–60].

B. Force and Torque on the Particle

In all our calculations below, we shall assume that the particle is fixed and calculate the forces on the particle. For the case of a moving particle, the slip velocity needs to be modified to account for the motion of the particle surface.

The total force and torque on any volume of the fluid are conveniently given in terms of the stress tensor, σ, by

$$\mathbf{F} = \int_{\partial\Omega} \mathbf{n} \cdot \sigma dA \tag{2}$$

$$\mathbf{T} = \int_{\partial\Omega} \mathbf{r} \times (\mathbf{n} \cdot \sigma) dA \tag{3}$$

The stress tensor contains contributions from electrical and viscous stresses on the fluid, $\sigma = \sigma_M + \sigma_H$, where

$$\sigma_M = \varepsilon[\mathbf{EE} - \frac{1}{2}E^2\mathbf{I}]$$
$$\sigma_H = -p\mathbf{I} + \eta\left(\nabla\mathbf{u} + (\nabla\mathbf{u})^T\right)$$

are the Maxwell and hydrodynamic stress tensors, respectively.

C. Particle Dynamics

In order to calculate the movement of a colloidal particle, we need to find a translational velocity $\mathbf{U}$, and a rotational velocity $\mathbf{\Omega}$ such that the net force on the particle is zero, when the slip velocity is modified by taking into account the velocities $\mathbf{U}$ and $\mathbf{\Omega}$. In other words, we are seeking $\mathbf{U}$ and $\mathbf{\Omega}$ such that the problem (1) with boundary condition

$$\mathbf{u} = \mathbf{u}_{slip} + \mathbf{U} + \mathbf{r} \times \mathbf{\Omega}$$

yields $\mathbf{F} = \mathbf{0}$ and $\mathbf{T} = \mathbf{0}$.

Since the Stokes problem is linear, there is a linear relationship between the translational and rotational motion of the particle and the resulting force and torque exerted on it by the fluid. Let us denote this relationship by

$$\begin{pmatrix} \mathbf{F} \\ \mathbf{T} \end{pmatrix} = \mathbf{M} \begin{pmatrix} \mathbf{U} \\ \mathbf{\Omega} \end{pmatrix}$$

The viscous hydrodynamic tensor $\mathbf{M}$ comes from solving for the Stokes flow around a particle moving with translational velocity $\mathbf{U}$ and rotational velocity $\mathbf{\Omega}$, assuming no slip on all particle and wall surfaces.

If we then solve the electrokinetic problem for a fixed particle in the applied field, we obtain the ICEO slip velocity $\mathbf{u}_{slip}$ as well as the total (hydrodynamic + electrostatic) force $\mathbf{F}_{slip}$ and torque $\mathbf{T}_{slip}$ needed to hold the particle in place, thereby preventing ICEP and DEP motion.

Using these calculations and invoking linearity, the condition of zero total force and torque on the particle, $\begin{pmatrix} \mathbf{F} \\ \mathbf{T} \end{pmatrix} + \begin{pmatrix} \mathbf{F}_{slip} \\ \mathbf{T}_{slip} \end{pmatrix} = 0$, determines the motion of the particle

$$\begin{pmatrix} \mathbf{U} \\ \mathbf{\Omega} \end{pmatrix} = -\mathbf{M}^{-1} \begin{pmatrix} \mathbf{F}_{slip} \\ \mathbf{T}_{slip} \end{pmatrix} \tag{4}$$

The particle trajectory is then described by the solution to the differential equation

$$\frac{d\mathbf{x}}{dt} = \mathbf{U}$$

together with the equations for the particle's angular orientation.

This angular orientation is irrevelant for a symmetric, fully polarizable or insulating particle. For the Janus particle, we will argue that only the rotations about $x-$axis are important, thus we will focus on the dynamics of just a single angle. In this case, the rotational equation of motion is simply

$$\frac{d\theta}{dt} = \Omega_x$$

D. Nondimensional Equations

We nondimensionalize the variables by

$$\mathbf{x}' = \frac{\mathbf{x}}{a}, \quad \phi' = \frac{\phi}{E_\infty a}, \quad \zeta' = \frac{\zeta}{E_\infty a}$$
$$q' = \frac{\varepsilon E_\infty a}{\lambda_D} q$$
$$t' = \left(\frac{\lambda_D a}{D}\right)^{-1} t, \; t'' = \left(\frac{\eta}{\varepsilon E_\infty^2}\right)^{-1} t$$
$$\mathbf{u}' = \mathbf{u}\left(\frac{\varepsilon E_\infty^2 a}{\eta}\right)^{-1}, \qquad p' = \frac{p}{\varepsilon E_\infty^2}$$

Note that there are two time scales in the problem, $\tau' = \frac{\lambda_D a}{D}$, the charging time, and $\tau'' = \frac{\eta}{\varepsilon E_\infty^2}$, the time scale for particle motion.

Plugging in the equations, we obtain (after dropping the primes except for t)

$$\nabla^2 \phi = 0, \quad \nabla^2 \mathbf{u} = \nabla p, \quad \nabla \cdot \mathbf{u} = 0 \tag{5}$$

with the boundary conditions

$$\frac{dq}{dt'} = \mathbf{n} \cdot \nabla \phi, \quad \mathbf{u} = \zeta \nabla_s \phi \tag{6}$$

on the particle surface, where $\zeta = \phi_{surface} - \phi_{bulk}$, is the zeta potential. For a polarizable particle, we have $\phi_{surface} = 0$ by symmetry, therefore we are left with $\zeta = -\phi_{bulk} = -\phi$. In addition, we have $\nabla\phi \sim \hat{\mathbf{x}}$, $|\mathbf{x}| \to \infty$, along with no slip on the planar wall zero flow at infinity. The linearized charge-voltage takes the simple form

$$q = -\zeta = \phi$$

The dimensionless force and torque on the particle are given by the formulae (2) and (3), where the stress tensors are replaced by their dimensionless counterparts

$$\sigma_M = \mathbf{EE} - \frac{1}{2} E^2 \mathbf{I}$$
$$\sigma_H = -p\mathbf{I} + \left(\nabla \mathbf{u} + (\nabla \mathbf{u})^T\right)$$

The force, angular momentum and stress tensors are scaled to

$$F_{ref} = \varepsilon E_\infty^2 a^2, \; T_{ref} = \varepsilon E_\infty^2 a^3, \; \sigma_{ref} = \varepsilon E_\infty^2$$

Finally, the particle motion is governed by

$$\frac{d\mathbf{x}}{dt''} = \mathbf{U}, \; \frac{d\theta}{dt''} = \Omega_x$$

E. Simplifications

1. Steady Problems

In some cases below, we consider a constant DC voltage, or a time-averaged AC steady state. This leads to Neumann boundary conditions on the cylinder or sphere. In that case

$$F_E = \int_{\partial\Omega} \left[\mathbf{E}(\mathbf{E}\cdot\mathbf{n}) - \frac{1}{2}E^2\mathbf{n}\right] dA = -\frac{1}{2}\int_{\partial\Omega} E^2 \mathbf{n} dA$$

because $\mathbf{E}\cdot\mathbf{n} = 0$ on the surface. As a consequence, the electrostatic torque induced on the particle is zero.

2. Symmetry

We adopt the coordinate system indicated in Fig. 1 where the field axis, parallel to the wall, is in the x direction. The problem simplifies considerably for symmetric particles and a symmetric electrolyte, as assumed in the linearized Standard Model considered here. (See Ref. [53] for a discussion of induced-charge electrokinetic phenomena resulting from broken symmetries in the electrolyte, such as different ion sizes, valences or mobilities.)

For the full cylinder problem, the electrostatic potential has an odd symmetry along the field axis, $\phi(x,z) = -\phi(-x,z)$, and for the full sphere problem, it also has even symmetry in the $y-$ direction, $\phi(x,y,z) = \phi(x,-y,z) = -\phi(-x,y,z)$. As a result, in both cases, E^2 has even symmetry in x and y. Therefore, in the steady case, electrostatic force (surface integral of $E^2\mathbf{n}$) vanishes in those directions, and there can only be a force in the z direction toward the wall.

In general time-dependent situations, the normal field $\mathbf{E}\cdot\mathbf{n}$ on the particle does not vanish, but it has odd symmetry in x and even symmetry in y. The axial field component E_x has even symmetry in both x and y, and (for a sphere) the transverse component E_y has even symmetry in x and odd symmetry in y. As a result, the surface integral of $\mathbf{E}(\mathbf{E}\cdot\mathbf{n}$ also vanishes in the x and y directions, again leaving an electrostatic force only in the z direction.

As for the flow problem, the electro-osmotic slip has the same symmetries as the tangential electric field. By similar arguments, this leads to flows that can only exert hydrodynamic forces in the z direction. Of course, many of these symmetries are broken for anisotropic Janus particles, as shown in Fig. 8 below.

3. AC fields

In the linear model we are considering, the time-periodic electrostatic forcing problem [35] can be solved by letting

$$\phi = \mathrm{Re}(\tilde{\phi} e^{i\omega t})$$

and solving for the complex potential $\tilde{\phi}$ using the equations

$$\nabla^2 \tilde{\phi} = 0$$

with the boundary conditions

$$n \cdot \nabla \tilde{\phi} = i\omega \tilde{\phi} \text{ (particle)}, \quad n \cdot \nabla \tilde{\phi} = 0 \text{ (wall)}$$

and $\tilde{\phi} \sim E_\infty x$ at ∞. In the high frequency limit, the electrostatic problem approaches the solution of the Dirichlet problem, since the first boundary condition is replaced by

$$\tilde{\phi} \to 0 \text{ (high frequency)} \tag{7}$$

because $\tilde{\phi} = n \cdot \nabla \tilde{\phi} / i\omega \to 0$. Physically, this means that the double layers do not have enough time to charge when the forcing frequency is too high.

Once the complex electrostatic potential is calculated, the time-averaged slip velocity can be obtained by the formula

$$\mathbf{u}_s = \frac{1}{2} \mathrm{Re}[\tilde{\zeta} \tilde{E}_\perp^*] \tag{8}$$

where $\tilde{\zeta}$ is the (complex) surface zeta potential, which is equal to $-\tilde{\phi}$ in the linear theory, and $\tilde{E}_\perp^*$ is the complex conjugate of the tangential component of $\tilde{E} = \nabla \tilde{\phi}$, the complex electric field. In the DC limit as $\omega \to 0$, the imaginary parts of the solutions go to zero, and we are left with $\mathbf{u}_s = \frac{1}{2} \zeta E_\perp$, which is the standard Smoluchowski's formula with a factor of $1/2$.

If the problem involves a fixed geometry, time averaging of the electrokinetic slip is a usual practice [35, 61–63] that is justified by the linearity of the Stokes equations. We also analyze the motion of Janus particles near walls later in this article, which involves time-dependent geometries, which might call the time-averaging of the equations into question. Since the particles do not move significantly within one period of AC forcing, however, it is still a good approximation to use time-averaged slip velocities. To see this, we compare the moving time scale a/U with the forcing period $1/\omega$. For example, in the experiments of Gangwal et al. [42], the parameters $a = 5.7\mu$m, $U < 30\mu$m/s, and $\omega = 1$ kHz, imply $U/a\omega < 0.006$. In other words, the AC period is roughly 200 times shorter than the time it takes the particle to translate by one radius. More generally,

$$\frac{U}{a\omega} \sim \frac{\varepsilon}{\eta} (\frac{kT}{ea})^2 \tau_c \approx 4 \times 10^{-5}$$

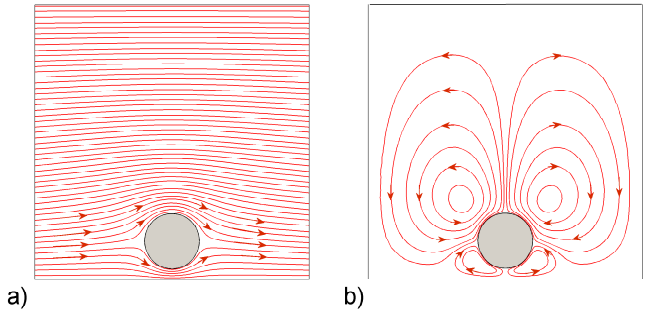

FIG. 2: Cylinder near a wall in a 10×10 box, in units of the diameter: (a) Electric field lines. (b) Stokes flow streamlines.

at a concentration of $c_0 = 1mM$, again with $a = 5.7\mu m$. If a compact layer is assumed, this figure is further divided by $(1 + \delta)$. Therefore, using the time-averaged slip will not result in lose of accuracy unless the AC forcing period is several orders of magnitude longer than the unit charging time.

F. Numerical Methods

We have solved the equations (in weak form) using the finite element software COMSOL (as in many previous studies of ICEO flows, e.g. [35, 62–66]). This allows us to handle complicated asymmetric geometries arising in the motion of Janus particles near walls below, but it requires placing the particle in a finite simulation box. As noted below, we have checked that increasing the box size does not significantly affect any of our results, and we have checked the numerical results against analytical solutions where possible.

For linear and nonlinear models alike, the computational efficiency is improved by first solving the electrostatic problem, and then the hydrodynamic problem. In time dependent cases, the fluid slip can be averaged and the Stokes problem is solved only once using this averaged slip.

In order to apply the finite-element method, the system of equations is converted to the weak form by multiplying by corresponding test functions and integrating over the spatial domain. The electrical problem turns into

$$\begin{aligned} 0 = -\int_\Omega \hat{\phi} \nabla^2 \phi d\mathbf{r} &= \int_\Omega \nabla \hat{\phi} \nabla \phi d\mathbf{r} + \int_{\partial\Omega} \hat{\phi} (\mathbf{n} \cdot \nabla \phi) ds \\ &= \int_\Omega \nabla \hat{\phi} \nabla \phi d\mathbf{r} + \int_{\partial\Omega} \hat{\phi} \partial_t \phi d\mathbf{r} \end{aligned}$$

which is satisfied for all test functions $\hat{\phi}$. The weak form

of the flow problem is similarly obtained as

$$0 = -\int_\Omega [\hat{\mathbf{u}} \cdot (\nabla \cdot \sigma) d\mathbf{r} + \hat{p} \nabla \cdot \mathbf{u}] d\mathbf{r}$$
$$= -\int_\Omega [\nabla \hat{\mathbf{u}} : \sigma - \hat{p} \nabla \cdot \mathbf{u}] d\mathbf{r} + \int_{\partial\Omega} \hat{\mathbf{u}} \cdot (\mathbf{n} \cdot \sigma)\, ds$$

where $\sigma = \sigma_H$ is the hydrodynamic stress tensor. Since we do not have a simple expression for $\mathbf{n} \cdot \sigma$, it is best to introduce the new variable (Lagrangian multiplier) $\mathbf{f} = \mathbf{n} \cdot \sigma$. This is also convenient for calculation of hydrodynamic forces at the surface. Then we obtain

$$0 = -\int_\Omega [\nabla \hat{\mathbf{u}} : \sigma - \hat{p} \nabla \cdot \mathbf{u}] d\mathbf{r} + \int_{\partial\Omega} [\hat{\mathbf{u}} \cdot \mathbf{f} + \hat{\mathbf{f}} \cdot (\mathbf{u} - \mathbf{u_s})] ds$$

In the problems analyzed in this paper, we have tested our numerical results for their dependence on the mesh parameters and the domain size and chosen these parameters accordingly in the final calculations. For example, for the Janus particle problem, the mesh parameters are: $h_{\max}^{surface}$, maximum mesh size on the particle surface; $h_{\max}^{global}$, maximum mesh size in the bulk; h_{narrow}, the COMSOL parameter for meshing narrow regions; and the dimensions of the domain: widths W_x, W_y, and height H. The other COMSOL mesh parameters are left unchanged at their default values. We have run our codes on nine different meshes, indexed by $k_{mesh} = 1, 2, .., 9$, with parameters $h_{\max}^{surface} = 0.4 - 0.025(k_{mesh} - 1)$, $h_{\max}^{global} = 7 - 0.5(k_{mesh} - 1)$, $h_{narrow} = 1.3 - 0.1(k_{mesh} - 1)$, $W_x = 6 + 3(k_{mesh} - 1)$, $W_y = H = 5 + 2.5(k_{mesh} - 1)$. At various Janus particle locations and orientations, there is less than 1 % difference between the calculated particle velocities and rotational speeds for the meshes $k_{mesh} = 5, 6, 7, 8, 9$. This agreement may deteriorate in relative terms when the comparison is made between quantities that approach zero, such as the translational or angular velocity for a Janus particle nearly facing the wall, however, the absolute differences always remain small. In the sections analyzing the isotropic spheres and the Janus particles, we report results obtained by using the most refined mesh, denoted here by $k_{mesh} = 9$.

III. ISOTROPIC PARTICLES NEAR A WALL

A. Cylinder in a DC Field

For isotropic particles near a wall, by symmetry, $\phi_{cylinder} = 0$, therefore $\zeta = -\phi$. Moreover, there is no net horizontal force exerted on the particle, so the only force of interest is in the vertical direction. Another consequence of symmetry is the absence of net torque on the cylinder.

The DC cylinder problem has been solved analytically by Zhao and Bau [52] in the linear case in bipolar coordinates. The mapping between the bipolar and the Cartesian coordinates is given by

$$x = \frac{c \sin\beta}{\cosh\alpha - \cos\beta}, \quad y = \frac{c \sinh\alpha}{\cosh\alpha - \cos\beta}$$

where $\alpha_0 < \alpha < \infty$, and $-\pi < \beta < \pi$ defines the region outside the cylinder. The geometric constants α_0 and c are defined as

$$\alpha_0 = \operatorname{sech}^{-1}\frac{a}{h}, \quad c = \frac{h}{\coth\alpha_0}$$

(Note that there is an error in the expression for α_0 in [52]). The hydrodynamic and electrostatic forces on the cylinder are calculated to be

$$F_H = \frac{2\pi \sinh\alpha_0 E_\infty^2 c}{(\alpha_0 \cosh\alpha_0 - \sinh\alpha_0)\coth\alpha_0} \times \left\{ \frac{1}{2\sinh^2\alpha_0} + \sum_{n=1}^{\infty} \left(\frac{\cosh\alpha_0}{\sinh(n+1)\alpha_0 \sinh\alpha_0} - \frac{1}{\sinh(n+2)\alpha_0 \sinh n\alpha_0} \right) \right\} \hat{\mathbf{y}}$$

$$F_E = \frac{2\pi E_\infty^2 h}{\coth\alpha_0} \sum_{n=1}^{\infty} \left(\frac{n^2}{\sinh^2 n\alpha_0} - \frac{n(n+1)\cosh\alpha_0}{\sinh n\alpha_0 \sinh(n+1)\alpha_0} \right) \hat{\mathbf{y}}$$

Due to symmetry, there is no force in the horizontal direction.

We have used this analytical solution to validate our numerical solutions in COMSOL using a maximum mesh size of 0.1 or less on the cylinder (relative to the particle radius). The absolute errors are very small, although in the regions of small velocity far from the cylinder, the relative error can be a few percent in a box of size 20x20, compared to the analytical solution in a half space. In a 40x40 box, however, the relative error is uniformly less than one percent.

B. Cylinder in an AC field

As the electric fields are screened quickly by the electrolyte, an AC field is usually preferred. Use of an AC electric field also prevents harmful reactions on electrodes, and enables experimentalists to go to higher applied voltage differences. Such higher voltages may be desirable if they lead to stronger electrokinetic effects of interest.

Far from the wall, the ICEO slip velocity around an ideally polarizable cylinder in an AC field was derived by Squires and Bazant [34], which takes the dimensionless form

$$\langle u_\theta \rangle = \frac{\sin 2\theta}{1 + \omega^2}.$$

We use this expression to calibrate our numerical code, and find excellent agreement far from the wall. This result shows that ICEO flow decays algebraically as ω^{-2} above the RC charging frequency. Since electrostatic forces do not decay in this limit, we may expect a change in behavior near the wall. At high frequency, there is not enough time for double-layer relaxation, so the electric field ressembles that of a conductor in a uniform dielectric medium.

An important observation is that the total hydrodynamic forces vanishes at higher frequencies whereas the

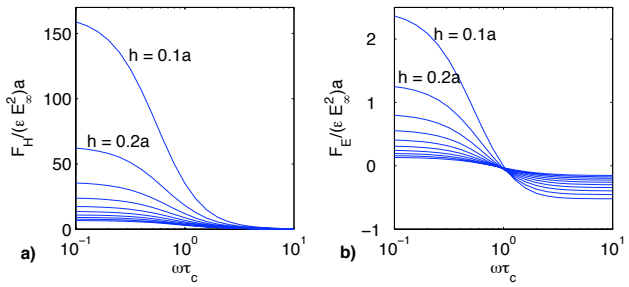

FIG. 3: The total (a) hydrodynamic (b) electrostatic forces on the cylinder as a function of AC frequency, at distances $h = 0.1ka$, $k = 1, 2, ..., 10$.

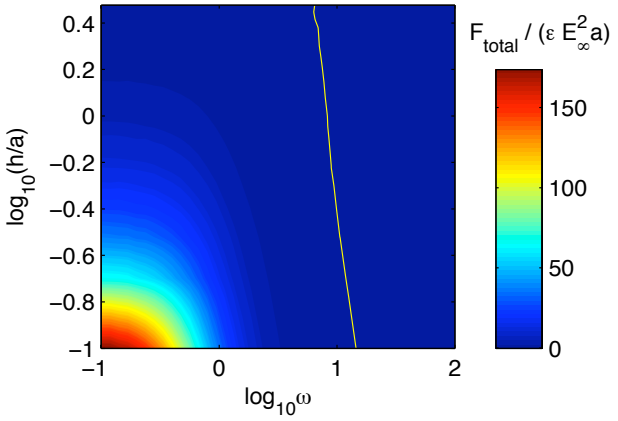

FIG. 4: Contour plot of total force on the ideally polarizable cylinder. There is an equilibrium distance between the cylinder and the wall at high enough frequencies, indicated by the yellow contour line. As the frequency is increased, this distance decreases.

total electrostatic force changes sign, but does not vanish. As a result, if the frequency is high enough, there is an equilibrium distance from the wall. This distance decreases as the frequency is increased.

In the high frequency limit, the electrostatic problem approaches the solution of the Dirichlet problem, that is, Laplace's equation, $\nabla^2\tilde{\phi} = 0$, with the boundary conditions, $\tilde{\phi} = 0$ on the cylinder, $n \cdot \nabla\tilde{\phi} = 0$ on the wall, and $\tilde{\phi} \sim -E_\infty x$ at ∞. As noted above, we introduce the complex potential[35], $\phi = \mathrm{Re}(\hat{\phi}e^{i\omega t}) = \hat{\phi}\cos\omega t$, and obtain an analytical solution,

$$\tilde{\phi} = 2cE_\infty \sum_{n=1}^{\infty} \frac{e^{-n\alpha_0}}{\cosh n\alpha_0} \cosh n\alpha \sin n\beta - \frac{c\sin\beta}{\cosh\alpha - \cos\beta}$$
$$= 2c\sum_{n=1}^{\infty}\left[\frac{e^{-n\alpha_0}}{\cosh n\alpha_0}\cosh n\alpha - e^{-n\alpha}\right]\sin n\beta$$

Plugging this into the electrostatic force leads to the formula

$$F_{E,\omega\to\infty} = -2\pi cE_\infty \sum_{n=1}^{\infty}\left(\frac{n^2}{\cosh^2 n\alpha_0} + \frac{n(n+1)\cosh\alpha_0}{\sinh n\alpha_0 \sinh(n+1)\alpha_0}\right)$$

with the same notation as in Zhao and Bau [52].

C. Sphere in an AC field

ICEO flow around a sphere was first considered by Gamayunov et al.[32]. Following the cylinder analysis of Squires and Bazant [34], it is straightforward to derive the (dimensionless) ICEO slip velocity around an ideally polarizable sphere in an AC field, far from the wall,

$$\langle u_\theta\rangle = \frac{9}{16}\frac{\sin 2\theta}{1+(\omega/2)^2} \tag{9}$$

Note that since $\langle\cos^2\omega t\rangle = 1/2$ the ICEO flow in a true DC field E_∞ is twice as large as the time-averaged flow in an AC field $E_\infty\cos\omega t$ in the low frequency or DC limit $\omega \to 0$. We will prefer reporting quantities for the DC limit throughout this chapter.

It is interesting to note (and unfortunate) that bispherical coordinates are not as helpful for the sphere-wall problem, as their two-dimensional analog is for the cylinder-wall problem analyzed above. For the electrostatic problem, there are semi-analytical solutions in our geometry [67–70], but they involve cumbersome series expansions, whose coefficients must be determined by numerically solving recursive equations. With a nontrivial electrostatic potential, the analytical solution to the fluid flow problem would be quite challenging, if not intractable, with all the broken symmetries of Janus particles near walls. Of course, an analytical solution to Laplace's equation for this geometry would be useful to resolve singularities accurately, but, even if possible, it may not be worth the mathematical effort, given the complex physics of very close particle-wall interactions, related to double layer overlap. As discussed below, the thin double layer approximation breaks down, before our numerical method breaks down, and closer overlaps require solving the full Poisson-Nernst-Planck equations, which is beyond the scope of this paper.

In the DC limit, the hydrodynamic and electrostatic forces on a sphere near a wall show qualitative similarity with that of a cylinder. As shown in Fig.5, both forces are repulsive and decay as the sphere moves away from the plane. Note that the magnitude of hydrodynamic forces are about 2 orders of magnitude larger than the dielectric forces.

The results start to differ from the cylinder problem for the case of real AC forcing, however. Shown in Fig.6 are the hydrodynamic and electrostatic forces as a function of AC frequency for a sphere at various distances

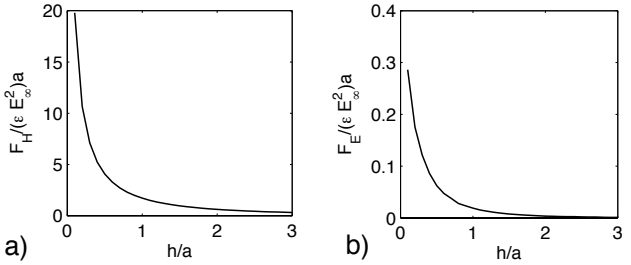

FIG. 5: The (a) hydrodynamic and (b) electrostatic forces on a full metal sphere in the DC limit as a function of the distance h from the wall.

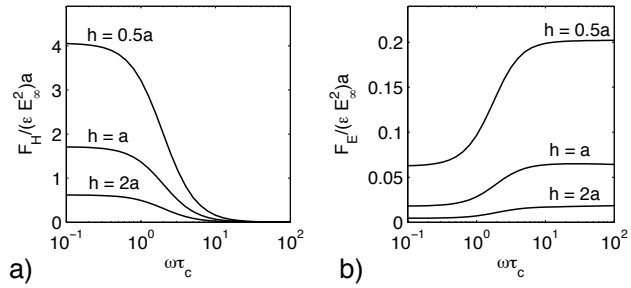

FIG. 6: The (a) hydrodynamic and (b) electrostatic forces on a full metal sphere as a function of frequency at the distances $h = 2a, a$, and $a/2$ away from the wall.

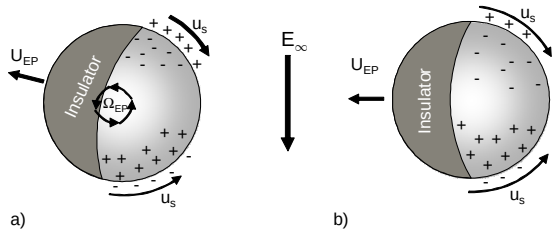

FIG. 7: A Janus sphere, initially tilted with respect to the electric field as in (a), would experience a hydrodynamic torque that aligns the equator of the Janus particle with the electric field as shown in (b).

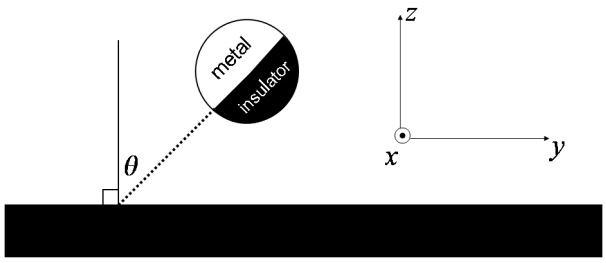

FIG. 8: Geometry of a Janus particle near the wall.

from the wall. While the hydrodynamic forces quickly drop to zero at high frequencies, the electrostatic forces persist and even increase at high frequencies, unlike the cylinder problem. Since both forces are repulsive, there is no equilibrium plane attracting the spherical particle, which is repelled to infinity by the wall regardless of the forcing frequency. This is true even when a Stern layer is introduced into the double layer model.

IV. JANUS SPHERE NEAR A WALL

A. Broken symmetries

Without a nearby wall, a Janus sphere would align itself perpendicular to the electric field. In other words, some of the electric field lines would be included in the plane dividing the Janus particle's metal and insulating sides. This effect has been studied by Squires and Bazant [38] and is illustrated in Fig. 7: If the Janus particle is initially tilted with respect to the electric field, the slip on its surface becomes nonuniformly distributed as the electric field has a larger tangential component on one side than the other. For example, in Fig. 7(a), there is a stronger slip on the lower metal surface. This results in a hydrodynamic torque that tends to align the particle perpendicular to the electric field.

The bulk rotation effect is presumably stronger than the wall effects, at least when the particle is sufficiently far from the wall. That being said, we will assume that the particle always stays in the described configuration, that is, with its dividing plane aligned with the electric field. This is not to say that the particle has no room for different rotational configurations because it can still rotate around x and y axis. By symmetry, there is no rotation about the $y-$ axis, so we are left with rotations only around the $x-$ axis. This is much easier to deal with than the original problem though, as only one angle is enough to describe the particles orientation.

Far from the wall, the bulk velocity perpendicular to a DC field in the stable orientation is given by the formula of Squires and Bazant [38] (Eq. 3.16), which takes the dimensionless form,

$$U_{DC} = \frac{9}{64} = 2\langle U_{AC}(\omega \to 0)\rangle \tag{10}$$

neglecting compact-layer surface capacitance. As noted above, the time-averaged velocity in a sinusoidal AC field is smaller by a factor of two in the limit of zero frequency.

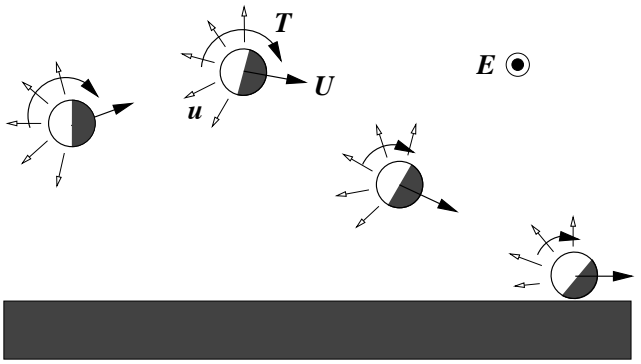

FIG. 9: Basic physics of Janus-particle-wall interactions. ICEO flows u in the plane perpendicular to the field (which is into the page) and the resulting ICEP torques T cause a Janus particle to tilt its less polarizable end toward a wall, while translating toward the wall (until stopped by double-layer overlap) and perpendicular to the applied AC field E (directed into the page and parallel to the wall). This physical mechanism may explain why the transverse ICEP motion of Janus particles was observable over the surface of a glass wall in the experiments of Gangwal et al. [42].

Even in the bulk, without a wall, it is difficult to solve analytically for the ICEO flow at finite AC frequency around a Janus particle, since the electrical response is not simply an induced dipole, due to the broken symmetry. Nevertheless, we will argue that the frequency dependence of the flow is similar to that around a sphere (9), constant below the RC charging time and decaying above it.

For a Janus sphere aligned perpendicular to the electric field near a wall, a crucial observation is that the $y-$symmetry breaks down. As a result, there is a net force in the $y-$direction, as well as a net torque in $x-$direction. The former leads to translation parallel to the wall, while the latter causes rotation of the dielectric face toward the wall. We shall see that these effects of broken symmetry completely change the behavior near wall in an AC or DC field: Although a polarizable sphere is always repelled to infinity by an insulating wall, a Janus particle is always (eventually) attracted to it.

B. Basic mechanism for wall attraction

The key new effect is rotation due to hydrodynamic torque caused by asymmetric ICEO flow near the wall. This generally causes the Janus particle to be attracted to the wall, as shown in figure 9. The physical mechanism can be understood as follows. When the field is first turned on, the Janus particle quickly rotates, by ICEP and DEP, to align its metal/insulator interface with the field axis, but with an arbitrary azimuthal angle, mainly set by the initial condition. As described by Squires and Bazant [38], the ICEO flow around the particle draws in fluid along the field axis and ejects it radially at the equator – but only on the polarizable hemisphere, which acts like a "jet engine" driving ICEP motion in the direction of the non-polarizable hemisphere.

Near a wall, as shown in the figure, the outward ICEO flow pushes down on the wall harder on the side of the polarizable "engine" than on that of the non-polarizable "nose", which produces a hydrodynamic torque tilting the nose toward the wall. A second cause of this rotation is the hydrodynamic coupling between ICEP translation parallel to the wall and rotation by shear stresses to cause rolling past the wall. Regardless of the initial position, these two sources of ICEP rotation cause the nose to eventually face the wall, so that the translational engine drives it toward the wall. This is likely the origin of the counter-intuitive attraction of Janus particles to a glass wall in the experiments of Gangwal et al [42].

What happens next depends on the details of the particle-wall interaction at very close distances. We will see that the bulk model with thin double layers must eventually break down, since the particle either collides with the wall or gets very close to it, leading to overlapping particle and wall double layers. It is beyond the scope of this work to accurately treat the nonlinear and time-dependent behavior of these overlapping double layers, so we will explore two models: (i) a cutoff "collision" height, where overlapping double layers stop any further motion toward the wall, while still allowing transverse motion, (ii) a compact-layer model (with dimensionless thickness, $\delta = 10$, defined below). Both cases use infinitely thin double layer approximation, that is, no overlapping double layers. The model (i) can be justified by the fact that, in the experiments [42], that the particles and walls have *equilibrium* surface charge of the same sign. For concreteness, we will simulate Model (i) with a cutoff height $h = \lambda = 0.05a$, e.g. corresponding to a double-layer thickness (screening length) of $\lambda = 50$nm with particles of size $a = 1\mu$m.

Based on examples above, we expect a subtle dependence on the AC frequency. Electrostatic DEP motion will always begin to dominate the hydrodynamic ICEP motion at high frequency. Therefore, we now consider the low and high frequency cases separately.

C. Dynamics as a function of AC frequency

As shown in Fig. 10, in the low frequency limit, the Janus particle experiences a rotational velocity turning its non-polarizable side toward the wall, as explained above. The hydrodynamic ICEP torque is orders of magnitude larger than the electrostatic DEP torque, until the particle gets quite close to the wall. The magnitude of the horizontal ICEP velocity U_y parallel to the surface and perpendicular to the field is close to its bulk value $U_y = 9/128 \approx 0.07$ even fairly close to the wall at a height $h = 0.5a$ at zero tilt, but reduces with the tilt angle. For small tilt angles and close to the wall at

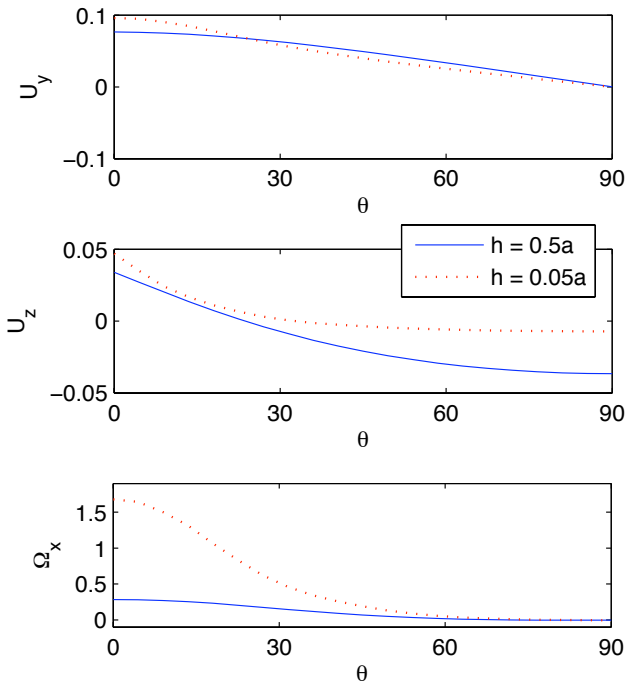

FIG. 10: In the DC limit ($\omega \to 0$), we plot (a) horizontal velocity (b) vertical velocity and (c) tilting speed (degrees/charging time) as a function of the tilt angle θ for the janus particle at distances $h = 0.5a$ and $h = 0.05a$ from the wall.

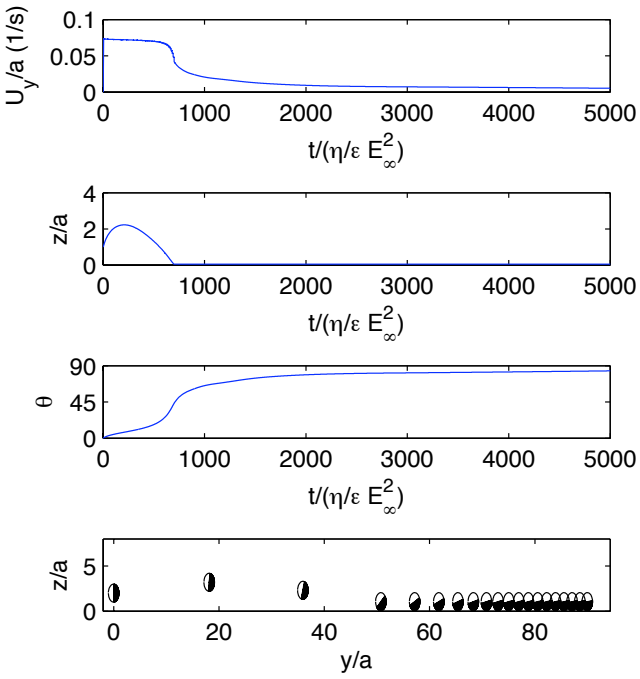

FIG. 11: Typical trajectory of a Janus particle under the DC limit $\omega \to 0$ interacting with the wall: As a function of time, plotted are (a) The horizontal speed (b) Distance from the wall (c) Tilt angle. Also, we plot the distance from the wall as a function of horizontal position in (d).

$h = 0.05a$, the horizontal velocity increases to $U_y \approx 0.10$, but it drops below the bulk value at larger tilt angles, e.g. to $U_y \approx 0.05$ at $\theta = 45$ degrees. Below we will see that this velocity is further reduced at higher forcing frequencies, due to the reduction of ICEO flow (since DEP cannot contribute to motion perpendicular to a uniform field).

If compact layer is absent, i.e. $\delta = 0$, in the DC limit the particle moves ever closer to the wall regardless of the orientation since $U_z < 0$ for any tilting of the nose toward the wall. Even if the the vertical motion is artificially stopped at a critical height, the rotation continues in the DC limit until the particle points its non-polarizable nose directly at the wall ($\theta = 90$) and the motion stops, although this can take a long time, since the rotation slows down substantially for tilt angles larger than 45 degrees. As discussed below, a number of effects might lead to such a stabilization of the tilt angle, thus allowing steady translation along the wall.

As shown in Fig. 11, a typical simulated trajectory of the Janus particle shows it translating perpendicular to the field while rotating and attracting to the wall, until eventually coming to rest facing the wall. Even when the particle's motion stops, however, its polarizable hemisphere ("engine") continues driving a steady ICEO flow, which can lead to long-range hydrodynamic interactions with other particles. This is an interesting theoretical prediction which should be checked in experiments. Such immobilized Janus particles may have interesting applications in microfluidics.

Similar behavior is predicted for finite AC frequencies in many cases. In particular, if a particle is initially mostly facing its non-polarizable hemisphere toward the wall (θ near 90°), it will swim toward the wall and come to rest, as in the DC limit of Figure 11.

There are some new effects in AC fields, however, since ICEO flows are suppressed with increasing frequency. The competing effect of DEP can prevent the Janus particle from fully rotating and coming to rest on the surface, at least in Model (i) where the collision is prevented artificially, as shown in Figure 12. At $\omega = 1$ (the characteristic RC frequency of the particle), the rotation slows down substantially beyond 45° but does not appear to stop. In this regime the horizontal velocity decays to $U_y \approx 0.015$. For $\omega = 10$ the particle appears to settle down to an equilibrium tilt angle around 45°, while steadily translating over the wall. The limiting horizontal velocity is roughly $U_y \approx 0.009$. As shown in Fig. 13, the rotational

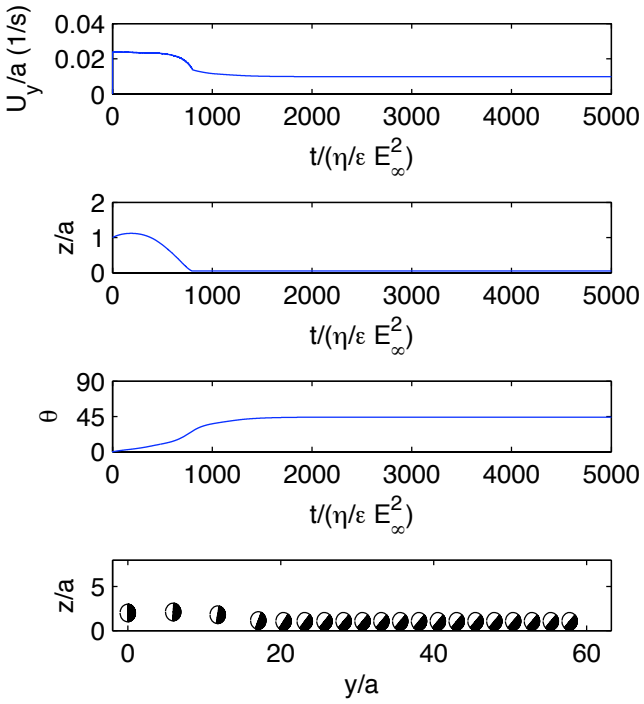

FIG. 12: Typical trajectory of a janus particle under AC frequency $\omega\tau_c = 10$ interacting with the wall: As a function of time, plotted are (a) The horizontal speed (b) Distance from the wall (c) Tilt angle. Also, we plot the distance from the wall as a function of horizontal position in (d).

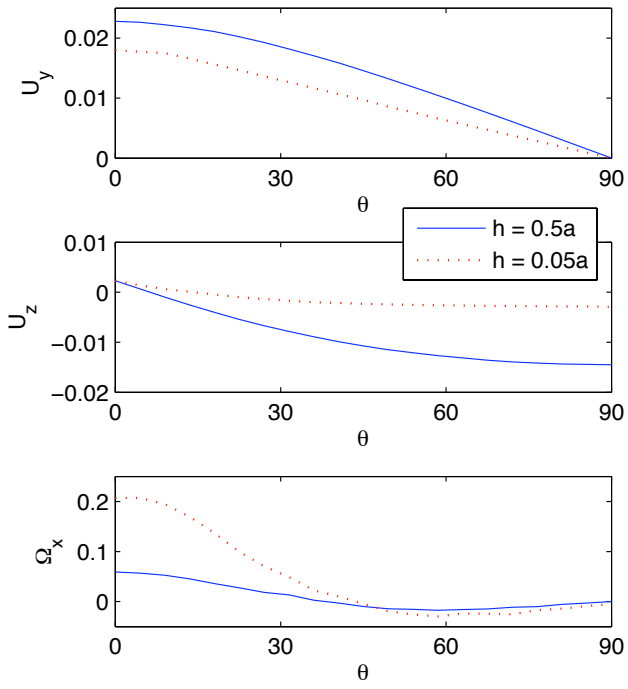

FIG. 13: For AC frequency ($\omega\tau_c = 10$), we plot (a) horizontal velocity (b) vertical velocity and (c) tilting speed (degrees/charging time) as a function of the tilt angle θ for the janus particle at distances $h = 0.5a$ and $h = 0.05a$ from the wall.

velocity has stable equilibrium angle already at $h = 0.5a$, which moving toward the wall, which becomes more pronounced at $h = 0.05a$, where the normal velocity nearly vanishes.

D. Compact-layer effects

At electrolyte interfaces, a molecular "compact layer" forms due to the adsorption of the solvent molecules and ions to the surface, which is considered to be outside the diffuse layer, where the continuum transport equations are still valid. The simplest theory for this compact layer is to assume a charge free region (which may consist of adsorbed solvent molecules) of an effective thickness λ_S that acts as a capacitance in series with the diffuse layer. This Stern layer model is crucial in explaining the behavior of the double layer capacitance when used with the Gouy-Chapman theory, which alone has unphysical predictions in the large voltage regime. (The effects of the compact layer can also be captured using modified models of the double layer for concentrated solutions [53].)

In electrophoresis, the compact layer model has been used extensively to explain the discrepancies between mathematical predictions and the experimental data. The key parameter is the dimensionless effective compact-layer thickness, $\delta = \lambda_S/\lambda_D$, scaled to the Debye length, which is also the ratio of the diffuse layer capacitance to the compact layer capacitance. Both the zeta potential and the electro-osmotic slip are reduced by the factor $1 + \delta$ under the classical assumptions of dilute-solution theory [53]. This results in a proportional decrease in the resulting hydrodynamic flow, which gives the main contribution to particle motion.

Without a compact layer, the predicted electrophoretic velocities are larger than the measured ones. Therefore (a positive) δ can be chosen to rescale the calculated quantities to match with the experiment. However, the compact layer model is more than just a simple scaling by $1/(1+\delta)$, because: (i) the electrostatic forces and motion induced by them are unaffected, (ii) the charging time and the characteristic AC frequency are also rescaled by $1/(1 + \delta)$.

In our model, the compact layer enables us to predict an equilibrium distance from the wall. For the particle facing the wall, there are two factors competing with each other; the hydrodynamic propulsion towards the wall and

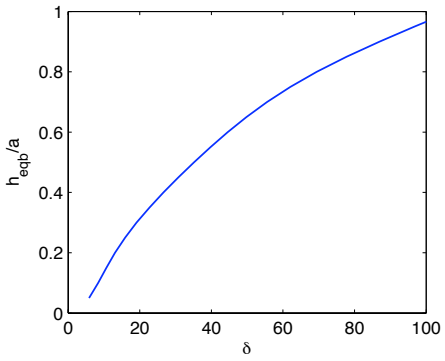

FIG. 14: Equlibrium distance from the wall versus the dimensionless ratio δ of the Stern length to the Debye length for a Janus particle in its equilibrium position in the electric field, directly facing the wall with its insulating side.

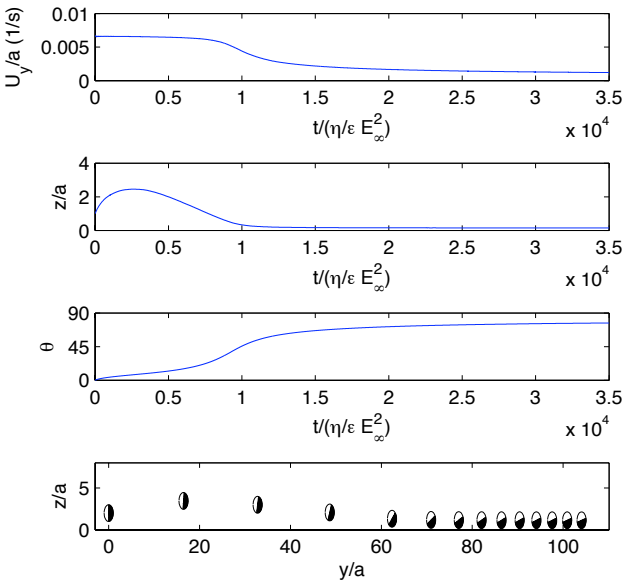

FIG. 15: Typical trajectory of a janus particle interacting with the wall in the limit $\omega \to 0$, with a compact layer of $\delta = 10$: As a function of time, plotted are (a) The horizontal speed (b) Distance from the wall (c) Tilt angle. Also, we plot the distance from the wall as a function of horizontal position in (d).

the electrostatic interaction pushing away from the wall. Both forces get stronger as the particle approaches the wall, as well as the ratio F_E/F_H of electrostatic force to hydrodynamic force. Still, even at small distances ($h = 0.05a$) from the wall, the attractive hydrodynamic force is 5-6 times larger than the repulsive electrostatic force.

Therefore the theory predicts that the particle eventually collides with the wall, which is contrary to what is observed in the experiments [42]. However, if we assume there is a compact layer with large enough δ, the hydrodynamic attraction can be made as small as the opposing electrostatic forces, and there exists an equilibrium distance for the particle. This equilibrium distance is an increasing function of δ, and it is plotted in Fig. 14.

As shown in Fig. 14, there is an equilibrium distance $h > 0.05a$ for the particle for $\delta > 5.7$ (simulations with smaller h are not well resolved). A choice of δ around 7-10 also helps us match the calculated horizontal electrophoretic velocities to experimentally measured values. Therefore the compact layer model explains the equilibrium distance from the wall while predicting particle velocities consistent with the experiment.

E. Comparison to experiment

Our simulations are in reasonable agreement with the experimental observations of Gangwal et al [42] for metallo-dielectric Janus particles in dilute NaCl solutions in the low-frequency regime $\omega < 1$. The bulk theory of Squires and Bazant (10) accurately fits the experimental velocity as a function of the field strength (Fig. 3 of Ref. [42]) and the particle size (Fig. 4), if $\delta = 10$, $U_{expt} = (9/128)/(1+10) = 0.006$. This $\delta-$value is somewhat larger than that inferred from prior experiments on ICEO flow in dilute KCl around a larger (100μm radius) platinum cylinder [35], but it is also observed that the ICEP velocity is slower than predicted at larger sizes (Fig. 4 of Ref. [42]). In addition, Gangwal et al [42] observed only the ICEP motion very close to the walls.

Our simulations predict that the particles are quickly attracted to the walls over a time of order the channel width (60 μm) divided by the typical ICEP velocity (1μm/s), which is roughly one minute, consistent with experimental observations. The particles are also predicted to tilt, and moderate tilt angles can also be inferred from experimental images, although more accurate measurements are needed. If the tilt angle stabilizes around 45° (see below), then the simulations (Fig. 10) predict that the ICEP translational velocity should be only $0.05/0.07 = 70\%$ of the bulk value close to the wall, which would imply the slightly smaller value $\delta = 7$. Apart from the rotational dynamics, therefore, the theory is able to predict the ICEP velocity fairly well.

Without stopping the rotation artificially, we are able to predict the experimentally observed steady motion along the wall only at moderate to large ω. The reduction of ICEO flow in this regime reduces hydrodynamic torque (see below) and also enhances the effect of stabilizing electrostatic forces. Although $U_{expt} = 0.006$ is measured in the low-frequency plateau $\omega < 1$, this behavior otherwise seems quite consistent, since the slower ICEP velocity can also fit the experimental data using smaller (and perhaps more reasonable) values of δ. For example, the predicted velocity of $U = 0.015$ at $\omega = 1$

implies $\delta = 1.5$, while the velocity $U = 0.009$ at $\omega = 10$ implies $\delta = 0.5$.

The difficulty in predicting the stable tilt angle at low frequency may be due to our use of the low-voltage, dilute-solution theory, which generally overpredicts the magnitude of ICEO flows, especially with increasing salt concentration. For example, the electrophoretic mobility can saturate at large induced voltages, and the charging dynamics can also be altered significantly when crowding effects are taken into account [53, 59]. As a result, our simulation results at moderate frequencies $\omega = 1 - 10$, which exhibit reduced ICEO flow due to incomplete double-layer charging, may ressemble the predictions of more accurate large-voltage, concentrated-solution theories at low frequency $\omega < 1$, where flow is reduced instead by ion crowding in the double layer [53].

Another open question relates to the observed decay of the motion with increasing bulk salt concentration c_b, which seems to be a universal feature of induced-charge electrokinetic phenomena, e.g. shared by AC electro-osmosis at micro-electrodes [71], and not captured by existing models [53, 59]. The experiments on ICEP of Janus particles show no concentration dependence below 0.1 mM NaCl and a steep decrease in velocity from 0.1 to 3 mM [42]. Above 5mM NaCl, still a rather dilute solution, the velocity becomes too small to measure accurately. In our model, the only source of concentration dependence is through ratio of diffuse-layer to Stern-layer capacitance, $\delta = C_D/C_S \propto \sqrt{c_b}$. this parameter enters (at low voltage) by rescaling the electro-osmotic slip velocity by $(1+\delta)^{-1} = (1+\sqrt{c_b/c_c})^{-1}$, where c_c is a crossover concentration. For $\delta > 1$ or $c_b > c_c$, the Stern layer carries most of the double-layer voltage, and the model predicts ICEO flow decreasing like $\sqrt{c_c/c_b}$ with increasing salt concentration. As described above, we find it necessary to fit the model to experiment at low concentrations with large values of $\delta > 1$, but this implies a concentration dependence like $\sqrt{c_c/c_b}$ for $c_b < 0.1$ mM, which is not observed. If instead we choose $c_c = 0.1$ mM, so that the concentration dependence sets in above this value (at the expense of greatly overpredicting velocities), the predicted decay with concentration in the model for $c_b > 0.1$ mM is still too weak to fit the data. It is clear that the standard model does not provide a complete description of ICEP, although it succeeds in explaining most of the qualitative phenomena observed in these experiments.

F. Contact mechanics

Another source of error in the model is our inaccurate treatment of the contact region, where double-layers may overlap. We have simply used the bulk thin-double-layer model for all our simulations, but there may be more complicated mechanical effects of the contact region. In particular, there may be enhanced hydrodynamic slip, due to the repulsion of overlapping (equilibrium) double layers of the same sign, as in the experiments.

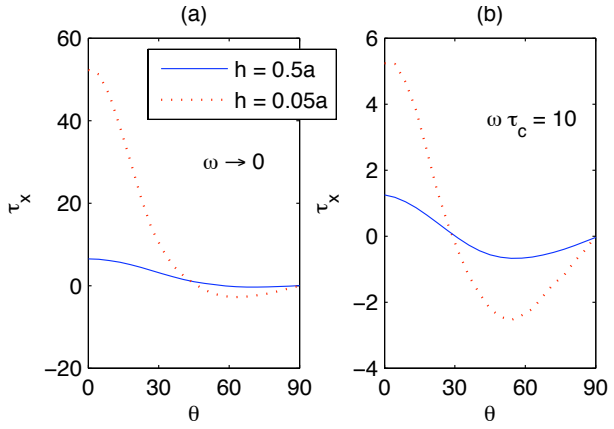

FIG. 16: Torque on a fixed Janus sphere versus tilt angle at heights $h = 0.5a$ and $0.05a$ when (a) $\omega \to 0$ (b) $\omega\tau_c = 10$.

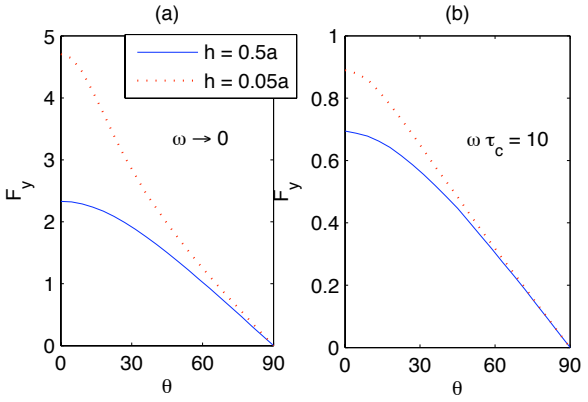

FIG. 17: Horizontal force on a fixed Janus sphere versus tilt angle at heights $h = 0.5a$ and $0.05a$ when (a) $\omega \to 0$ (b) $\omega\tau_c = 10$.

By examining the forces and torques close to the wall, we can infer to some degree what mechanical properties of the contact region might lead to the observed ICEP sliding along the wall and smaller tilt angles at lower frequencies (and thus also somewhat larger velocities). As shown in Fig. 16, before the particle gets very close to the wall, the (mostly hydrodynamic) torque acts to completely tilt the non-polarizable face toward the wall leading to collision. As noted above in Fig. 9, this can be understood as a result of the downward component of ICEO flow on the polarizable hemisphere raising the pressure by pushing on the wall on that side.

The situation changes when the particle gets very close to the wall. As shown in Fig. 16, the torque changes sign at a tilt angle which is roughly 45°. This again can be understood from Fig. 9, since the ICEO flow between the particle and the wall on the polarizable side, which drives the torque, is mostly absent. It would thus seem

that even in a DC field, the particle would not rotate any further, but this thinking neglects the hydrodynamic coupling between translational force and rotational velocity near the wall, Eq. (4). In Fig. 17, we see that the force on the particle parallel to the wall F_y remains strong, and this leads to a rolling effect over the wall due to shear stresses. For this reason, the rotational velocity persists in Fig. 10 even when the torque goes to zero in Fig. 16.

The model assumes no slip on all non-polarizable surfaces, but this may not be a good approximation near the contact point when double layers overlap. If the equilibrium surface charges (or zeta potentials) on the non-polarizable hemisphere and the wall have opposite signs, then the overlapping double layers lead to a strong attraction, which would only stiffen the effective contact with the surface, and thus only increase the viscous rolling effect during motion along the surface. If the equilibrium surface charges (or zeta potentials) have the same sign, however, as in the experiments on gold-coated latex Janus particles near glass walls [42], then there is a strong repulsion at the contact point. This repulsion stops the collision with the wall in Model (i), but it may also "lubricate" the contact and allow for some sliding. This effective slip over the wall near the contact point could reduce the viscous rolling, and, in the absence of torque, cause the rotation to stop, or at least be reduced for tilt angles above 45°. In that case, we might expect a more accurate model of the contact region to predict the experimentally observed motion, sliding over the surface by ICEP with a small tilt angle ($\theta < 45°$), for a wider range of conditions, including lower AC frequency, perhaps even in the DC limit.

V. CONCLUSION

We have used the existing low-voltage theory of ICEP to predict the motion of polarizable particles near an insulating wall. Our results for symmetric spheres and cylinders confirm the expected repulsion from the wall due to ICEO flow, sketched in Figure 1(a). In the case of the cylinder we show that attraction is also possible at high frequency, where DEP from electrostatic forces dominates slip-driven ICEP motion.

Our results for asymmetric Janus particles reveal an unexpected attraction to the wall by a novel mechanism illustrated in Figure 9, which involves tilting of the less polarizable face toward the wall. Once it gets very close to the wall ($h < a$), the particle either rotates completely to face the wall and ceases to move, while driving steady ICEO flow, or reaches an equilibrium tilt angle around 45° while steadily translating along the surface, perpendicular to the electric field. The latter motion only arises at moderate frequencies in our model, above the characteristic charging frequency for the double layers, while in experiments it is also observed at low frequencies. More accurate models taking into account reduced ICEO flow at large voltage in non-dilute solutions [53] and more accurate models of the contact region may improve the agreement with experiments.

In any case, we have shown that polarizable particles can display complex interactions with walls due to broken symmetries in ICEO flows. Attractive and repulsive interactions can be tuned by varying the geometry of the particles (and the walls), as well as the AC frequency and voltage. These remarkable phenomena may find applications in separation or self-assembly of colloids or in local flow generation in microfluidic devices [29, 46].

VI. ACKNOWLEDGEMENTS

This work was supported by the National Science Foundation under Contract No. DMS-0707641. M.Z.B. also acknowledges support from ESPCI through the Paris-Sciences Chair.

[1] J. L. Anderson, Annu. Rev. Fluid Mech. **21**, 61 (1989).
[2] J. Lyklema, *Fundamentals of Interface and Colloid Science. Volume II: Solid-Liquid Interfaces* (Academic Press Limited, San Diego, CA, 1995).
[3] R. J. Hunter, *Foundations of Colloid Science* (Oxford University Press, Oxford, 2001).
[4] W. B. Russel, D. Saville, and W. R. Schowalter, *Colloidal Dispersions* (Cambridge University Press, Cambridge, England, 1989).
[5] F. A. Morrison and J. J. Stukel, J. Colloid and Interface Science **33**, 88 (1970).
[6] H. J. Keh and J. L. Anderson, J. Fluid Mech. **153**, 417 (1985).
[7] H. J. Keh and S. B. Chen, J. Fluid Mech. **194**, 377 (1988).
[8] H. J. Keh, K. D. Horng, and J. Kuo, J. Fluid Mech. **231**, 211 (1991).
[9] H. J. Keh and J. S. Jan, J. Colloid Interface Science **183**, 458 (1996).
[10] J. Ennis and J. L. Anderson, J. Colloid Interface Science **185**, 497 (1997).
[11] A. L. Zydney, J. Colloid Interface Science **169**, 476 (1995).
[12] E. Lee, J.-W. Chu, and J.-P. Hsu, J. Colloid Interface Science **196**, 316 (1997).
[13] E. Lee, J. W. Chu, and J.-P. Hsu, J. Colloid Interface Science **205**, 65 (1998).
[14] A. A. Shugai and S. L. Carnie, J. Colloid Interface Science **213**, 298 (1999).
[15] M.-H. Chih and J.-P. Hsu, J. Colloid Interface Science **248**, 383 (2002).
[16] H. Liu, H. H. Bau, and H. H. Hu, Langmuir **20**, 2628 (2004).
[17] J.-P. Hsu and M.-H. Ku, J. Colloid Interface Sci. **283**, 592 (2005).
[18] S. M. Davison and K. V. Sharp, J. Colloid Interface Science **303**, 288 (2006).

[19] J.-P. Hsu, L.-H. Yeh, and Z.-S. Chen, J. Colloid Interface Sci. **310**, 281 (2007).
[20] J.-P. Hsu, Z.-S. Chen, M.-H. Ku, and L.-H. Yeh, J. Colloid Interface Sci. **314**, 256 (2007).
[21] E. Yariv, Phys. Fluids **18**, 031702 (2006).
[22] J.-P. Hsu, L.-H. Yeh, and M.-H. Ku, J. Colloid Interface Sci. **305**, 324 (2007).
[23] J. L. Anderson, J. Colloid Interface Science **105**, 45 (1984).
[24] M. C. Fair and J. L. Anderson, Langmuir **8**, 2850 (1992).
[25] D. Long and A. Ajdari, Electrophoresis **17**, 1161 (1996).
[26] D. Long and A. Ajdari, Phys. Rev. Lett. **81**, 1529 (1998).
[27] Y.-P. Tang, M.-H. Chih, E. Lee, and J.-P. Hsu, J. Colloid Interface Sci. **242**, 121 (2001).
[28] G. C. Randall and P. S. Doyle, Macromolecules **38**, 2410 (2005).
[29] M. Z. Bazant and T. M. Squires, Current Opinion in Colloid and Interface Science **15**, 203 (2010).
[30] M. Z. Bazant, in *Electrokinetics and Electrohydrodynamics of Microsytems*, edited by A. Ramos (Springer, in press), lecture notes on "Induced-charge electrokinetic phenomena" from CISM Summer School, Udine, Italy, June 2009.
[31] V. A. Murtsovkin, Colloid Journal **58**, 341 (1996).
[32] N. I. Gamayunov, V. A. Murtsovkin, and A. S. Dukhin, Colloid J. USSR **48**, 197 (1986).
[33] M. Z. Bazant and T. M. Squires, Phys. Rev. Lett. **92**, 066101 (2004).
[34] T. M. Squires and M. Z. Bazant, J. Fluid Mech. **509**, 217 (2004).
[35] J. A. Levitan, S. Devasenathipathy, V. Studer, Y. Ben, T. Thorsen, T. M. Squires, and M. Z. Bazant, Colloids and Surfaces A **267**, 122 (2005).
[36] A. J. Pascall and T. M. Squires, Phys. Rev. Lett **104**, 088301 (2010).
[37] E. Yariv, Phys. Fluids **17**, 051702 (2005).
[38] T. M. Squires and M. Z. Bazant, J. Fluid Mech. **560**, 65 (2006).
[39] D. Saintillan, E. Darve, and E. S. G. Shaqfeh, Journal of Fluid Mechanics **563**, 223 (2006).
[40] K. A. Rose and J. G. Santiago, Physical Review E **75**, 197 (2006).
[41] V. A. Murtsovkin and G. I. Mantrov, Colloid J. USSR **52**, 933 (1990).
[42] S. Gangwal, O. J. Cayre, M. Z. Bazant, and O. D. Velev, Phys. Rev. Lett. **100**, 058302 (2008).
[43] M. S. Kilic and M. Z. Bazant, arXiv:0712.0453v1 **[cond-mat.mtrl-sci]** (2007).
[44] Z. Wu, Y. Gao, and D. Li, Electrophoresis **30**, 773 (2009).
[45] Z. Wu and D. Li, Electrochimica Acta **54**, 3960 (2009).
[46] D. C. Prieve, P. J. Sides, and C. L. Wirth, Current Opinion in Colloid and Interface Science **15**, 160 (2010).
[47] M. Trau, D. A. Saville, and I. A. Aksay, Langmuir **13**, 6375 (1997).
[48] S. Yeh, M. Seul, and B. Shraiman, Nature (London) **386**, 57 (1997).
[49] P. J. Sides, Langmuir **17**, 5791 (2001).
[50] W. D. Ristenpart, I. A. Aksay, and D. A. Saville, Phys. Rev. Lett. **90**, 128303 (2003).
[51] W. D. Ristenpart, I. A. Aksay, and D. A. Saville, J. Fluid Mech. **575**, 83 (2007).
[52] H. Zhao and H. H. Bau, Langmuir **23**, 4053 (2007).
[53] M. Z. Bazant, M. S. Kilic, B. Storey, and A. Ajdari, Advances in Colloid and Interface Science **152**, 48 (2009).
[54] M. Z. Bazant, K. Thornton, and A. Ajdari, Phys. Rev. E **70**, 021506 (2004).
[55] Y. K. Suh and S. Kang, Phys. Rev. E **77**, 011502 (2008).
[56] Y. K. Suh and S. Kang, Phys. Rev. E **79**, 046309 (2009).
[57] M. S. Kilic, M. Z. Bazant, and A. Ajdari, Phys. Rev. E **75**, 033702 (2007).
[58] M. S. Kilic, M. Z. Bazant, and A. Ajdari, Phys. Rev. E **75**, 034702 (2007).
[59] M. Z. Bazant, M. S. Kilic, B. D. Storey, and A. Ajdari, New Journal of Physics **11**, 075016 (2009).
[60] A. S. Khair and T. M. Squires, Journal of Fluid Mechanics **640**, 343 (2009).
[61] N. G. Green, A. Ramos, and H. Morgan, J. Appl. Phys. D **33**, 632 (2000).
[62] M. Z. Bazant and Y. Ben, Lab on a Chip **6**, 1455 (2006).
[63] J. P. Urbanski, J. A. Levitan, D. N. Burch, T. Thorsen, and M. Z. Bazant, Journal of Colloid and Interface Science **309**, 332 (2006).
[64] G. Yossifon, I. Frankel, and T. Miloh, Phys. Fluids **19**, 068105 (2007).
[65] M. M. Gregersen, F. Okkels, M. Z. Bazant, and H. Bruus, New Journal of Physics **11**, 075016 (2009).
[66] M. M. Gregersen, M. B. Andersen, G. Soni, C. Meinhart, and H. Bruus, Phys. Rev. E **79**, 066316 (2009).
[67] A. Goyette and A. Navon, Phys. Rev. B **13**, 4320 (1976).
[68] R. D. Stoy, J. Appl. Phys. **65**, 2611 (1989).
[69] R. D. Stoy, J. Appl. Phys. **65**, 5093 (1989).
[70] P. C. Chaumet and J. P. Dufour, J. Electrostatics **43**, 145 (1998).
[71] V. Studer, A. Pépin, Y. Chen, and A. Ajdari, Analyst **129**, 944 (2004).